On the Coupling Number and Characteristic Length of Micropolar Media of Differing Topology

M. McGregor & M. A. Wheel

Department of Mechanical and Aerospace Engineering
University of Strathclyde
Glasgow, G1 1XJ, UK

marcus.wheel@strath.ac.uk
Tel +44 141 548 3307
Fax +44 141 552 5105

Abstract

In planar micropolar elasticity theory the degree of micropolarity exhibited by a loaded heterogeneous material is quantified by a dimensionless constitutive parameter, the coupling number. Theoretical predictions of this parameter derived by considering the mechanical behaviour of regular, two dimensional lattices with straight connectors suggest that its value is dependent on the connectivity or topology of the lattice with the coupling number in a square lattice predicted to be noticeably higher than in its hexagonal counterpart. A second constitutive parameter reflecting the intrinsic lattice size scale, the characteristic length, is also predicted to be topology dependent. In this paper we compare the behaviour of alternative two dimensional heterogeneous materials in the context of micropolar elasticity. These materials consist of periodic arrays of circular voids within a polymeric matrix rather than a lattice of straight connectors. Two material variants that differ only in their matrix topology are investigated in particular. Values of the additional micropolar constitutive parameters are obtained for each material from both experimental tests and finite element analyses. The values determined for these parameters, particularly the coupling number, suggest that their topological dependence differs appreciably from the theoretical predictions of the lattice models.

Keywords:

Micropolar elasticity, Cosserat elasticity, size effect, constitutive properties, characteristic length, coupling number.

1.0 Introduction

Higher order elasticity theories are believed to describe the behaviour of loaded heterogeneous materials since they acknowledge that the nature of the underlying microstructure influences overall mechanical response. This is particularly important when microstructural size scale approaches the overall scale. Classical or Cauchy elasticity theory does not acknowledge the effect of microstructure and is therefore unable to predict some of the more intriguing behaviour exhibited by heterogeneous materials such as the dependence of stiffness on size, the dispersion of propagating elastic waves and the dependence of stress concentrations or intensities on the sizes of the discontinuities producing them. In general terms higher order theories acknowledging microstructural influence have evolved by enhancing first order, classical theory through the incorporation of either strain, or sometimes stress, gradients or by incorporating additional, independent degrees of freedom. These two approaches are systematically compared by Tekoglu and Onck (2008) with the latter being adopted in micropolar or Cosserat elasticity where an independent rotational degree of freedom, the microrotation, augments the conventional displacement degrees of freedom of classical elasticity. Associated with the microrotation is an additional stress quantity, the couple stress, which is related to microrotation derivatives or curvatures through an additional constitutive parameter, the couple modulus, which in turn can be related to the conventional moduli governing dilatational and distortional deformation through a length scale parameter, the characteristic length, a further constitutive parameter common to many higher order theories. The presence of the couple stresses acting on a material element relaxes the symmetry requirement imposed on orthogonal shear stresses, they need no longer be complementary since any imbalance can be redressed by the couple stresses. The level of shear stress asymmetry is quantified by a further constitutive parameter, the coupling number, thereby reflecting the degree of micropolarity exhibited by the material. The coupling number is dimensionless but not independent since it can be expressed in terms of other constitutive parameters. Additionally, its range is bounded, the lower bound being the classically elastic case while at the upper bound the microrotation is equal to the conventional rotation, a case usually referred to as couple stress elasticity or sometimes constrained Cosserat elasticity.

While the bounds on the coupling number can be determined from energetic constraints, identifying likely values for genuinely micropolar materials is more challenging. One theoretically based approach is to consider the behaviour of a heterogeneous material that can be represented by a regular, periodic lattice of elastic connectors or elements. The lattice elements are usually straight, of uniform cross section, connected at their ends only and all of the same length. The elements may possess only axial or, in addition, bending and possibly transverse shear stiffness. One motivation for investigating such structures is to understand the likely behaviour of materials at an atomic or crystal lattice scale. The notion of representing a material in this manner dates back at least as far as Hrennikoff (1941) if not earlier. A comprehensive review of such investigations throughout the twentieth century is provided by Ostoja Starzewski (2002). The approach that is usually adopted in determining the behaviour of the material is to firstly establish the static mechanical response of some unit cell representing a portion of the lattice. This is normally achieved through total potential energy based arguments as adopted by for instance by Askar and Cakmak (1968), although a direct, matrix displacement type approach as utilized by for example Wang and Stronge (1999) is also applicable. The equivalence of these two approaches is indicated by Bažant and Christiansen (1972). Once the response of a unit cell has been identified the constitutive behaviour of the continuous material that the lattice purports to represent is then determined by a homogenization process. The relevant constitutive parameters can then be ascertained

from the behaviour thus determined. Noor and Nemeth (1980) and others indicate that an additional motivation for equating the behaviour of lattices to that of higher order continua is in analysing large scale loaded structures with regular, repeated elements when access to digital computing facilities on which to perform the necessary structural analysis by numerical means such as the finite element method is unavailable. This motivation may have been relevant when such facilities were not widespread and although it now appears obsolete, arguably it may still have some relevance in situations where expertise in utilizing finite element based structural analysis software is unavailable. It is also currently relevant in analysing those materials possessing intrinsically three dimensional heterogeneity where the explicit representation of the microstructure by a finite element discretization results an analysis that would challenge all but the most advanced of present day high performance computing facilities. A third motivation for investigating lattices is to provide a means of determining the behaviour of fabricated materials with a periodic structure discernible at the macro scale such as composites and metallic and polymeric cellular honeycomb materials in which the geometry of the microstructure is in essence defined in two dimensions and simply extruded in the third direction. Such materials are now being exploited extensively in applications such as sandwich panel construction techniques because of the weight saving opportunities they afford. Thus two dimensional hexagonal lattice structures representative of honeycombs have been investigated by amongst others Gibson and Ashby (1997) and Wang and Stronge (1999) with expressions for the equivalent or micropolar modulus being derived in terms of the element constitutive properties and geometry. Spadoni and Ruzzene (2012) provide a consistent list of expressions for the additional micropolar constitutive properties, namely the characteristic length and coupling number, of square, equilateral triangular and hexagonal lattice structures in terms of the element length and thickness, the list being based on the previous work of Banks and Sokowlowski (1968), Dos Reis and Ganghoffer (2011) and Wang and McDowell (2004). Pertinent to this work are the expressions for the characteristic length and in particular the coupling number of materials with square and hexagonal lattices since they imply that for a given element thickness to length ratio there will be a noticeable difference in these additional properties between these material types. Suiker et al. (2001) considered the effect of lattice topology on the constitutive parameters but in the dynamic rather than static case. They concluded that as the macroscopic lengthscale, quantified by wavelength, is reduced towards the microscopic lengthcale associated with the lattice the agreement between the lattice model and the micropolar continuum description diminishes because the characteristic length parameter becomes increasingly more sensitive to lattice topology. Chung and Waas (2009) investigated the behaviour of a specific hexagonally packed polycarbonate honeycomb comprised of circular rather than polygonal cells. This particular honeycomb has some resemblance to one of the materials considered here, the difference being that the honeycomb contains additional triangular shaped voids in the interstices between neighbouring cells. Using a combination of finite element and dimensional analysis of a representative volume they obtain expressions for the compliances of the honeycomb. The analysis assumes constrained micropolar behaviour since the microrotation is set equal to the macrorotation and as a consequence the derived value of the micropolar compliance is zero. Bigoni and Drugan (2007) considered the case of a heterogeneous material comprised of compliant circular inclusions within an isotropic matrix. When the inclusions are more compliant than the matrix the material exhibits Cosserat like behaviour and an analytical expression for the characteristic length is derived for the limiting case where the inclusions are voids.

The additional constitutive parameters of micropolar elastic materials can also be determined experimentally by loading them and observing the resulting deformation. The customary

approach, summarized by Lakes (1995), exploits the size effect forecast for such materials by attempting to measure the expected variation in stiffness with material sample size. In this method of size effects the constitutive parameters are then derived by interpretation of the observed variation using a known, usually closed form analytical, solution specific to the sample geometry and loading mode employed. This approach was successfully utilized by Yang and Lakes (1982) and Lakes (1983, 1986) to determine the micropolar constitutive properties of biological and fabricated materials respectively. The need for careful sample preparation was emphasised by Anderson and Lakes (1994) since any retained surface damage would result in increased compliance that would corrupt the observed size effect. Moreover, since the scale of the heterogeneity in the materials investigated often necessitated the testing of small samples, Lakes (1995) advocated loading by electromagnetic means or dead weights in order to negate friction and contact effects associated with conventional mechanical loading which would also compromise results. Lakes (1995) acknowledges that despite attempting to circumvent these effects data obtained from small samples is nonetheless still subject to error and recourse to numerical methods may be required to minimize the deviation between measured data and known solution if values for the additional elastic constants, particularly the coupling number, are to be identified reliably. Beveridge et al. (2013a) subsequently applied the method of size effects in investigating the behaviour of a material consisting of an aluminium alloy matrix perforated by a regular array of circular voids. The identified behaviour was successfully interpreted within the context of micropolar elasticity using a simplification of the analytical solution for the deflection of a loaded rectangular sectioned micropolar beam, quoted by Lakes (1995), to determine the characteristic length of the material. The scale of the heterogeneity introduced into the matrix was deliberately chosen to facilitate loading on conventional mechanical testing equipment. The variation in stiffness with sample size was also measured at a reduced slenderness where shear deformation would be more significant. The coupling number was then identified from this variation by an inverse approach based upon minimizing the difference between experimental measures of stiffness and predictions obtained from a numerical finite element analysis in which the coupling number could be adjusted. Beveridge et al. (2013a) argue that the deliberate creation, testing and analysis of such a material is more than simply didactic; the consistency of the constitutive property data obtained through independent testing and finite element analysis reinforces the credibility of the size effect methodology in the more challenging case of materials with genuinely three dimensional heterogeneity where only an experimental approach is viable since analysis is presently unrealizable in practice for the reasons already outlined. Acknowledging this Waseem et al. (2013) employed a similar approach albeit in a circular ring sample geometry rather than a straight beam to identify size effects in a material comprised of an acrylic polymer matrix with the same topology. For consistency, micropolar elasticity theory was again used to translate the observed effects into the relevant constitutive properties; the characteristic length and coupling number. Interestingly, the value for the characteristic length when normalized with respect to the scale of the heterogeneity, which was significantly smaller in the ring samples, was comparable to that obtained by Beveridge et al. (2013a) for the beam samples while the value of the coupling number identified was also remarkably similar. These comparisons, establishing the effect of geometric scaling and matrix modulus on both the characteristic length and coupling number parameters, accord with the predictions of lattice models. Such models also predict that these constitutive parameters will depend on the connectivity of the lattice elements. In this paper the veracity of this further prediction to the perforated materials is considered by examining the effect that altering the matrix topology has upon the parameters.

2.0 Constitutive Behaviour of Micropolar Elastic Materials and the Role of the Coupling Number

In the two dimensional plane stress case the constitutive equations of a linear, isotropic micropolar material introduced by Eringen (1966, 1999):-

$$\tau_{ij} = \lambda \varepsilon_{kk} \delta_{ij} + \left(2\mu^* + \kappa\right)\varepsilon_{ij} + \kappa e_{ijk}\left(\theta_k - \phi_k\right) \qquad (1)$$

$$m_{ij} = \alpha \phi_{k,k} \delta_{ij} + \beta \phi_{i,j} + \gamma \phi_{j,i} \qquad (2)$$

can be expressed in the form:-

$$
\begin{bmatrix} \tau_{xx} \\ \tau_{yy} \\ \tau_{xy} \\ \tau_{yx} \\ m_{xz} \\ m_{yz} \end{bmatrix}
= \frac{E_M}{\left(1 - v_M^2\right)}
\begin{bmatrix}
1 & v_M & 0 & 0 & 0 & 0 \\
v_M & 1 & 0 & 0 & 0 & 0 \\
0 & 0 & \dfrac{\left(1 - v_M\right)}{2\left(1 - N^2\right)} & \dfrac{\left(1 - v_M\right)\left(1 - 2N^2\right)}{2\left(1 - N^2\right)} & 0 & 0 \\
0 & 0 & \dfrac{\left(1 - v_M\right)\left(1 - 2N^2\right)}{2\left(1 - N^2\right)} & \dfrac{\left(1 - v_M\right)}{2\left(1 - N^2\right)} & 0 & 0 \\
0 & 0 & 0 & 0 & 2l_b^2\left(1 - v_M\right) & 0 \\
0 & 0 & 0 & 0 & 0 & 2l_b^2\left(1 - v_M\right)
\end{bmatrix}
\begin{bmatrix} \varepsilon_{xx} \\ \varepsilon_{yy} \\ \varepsilon_{xy} \\ \varepsilon_{yx} \\ \phi_{z,x} \\ \phi_{z,y} \end{bmatrix}
$$

$$(3)$$

according to Lakes and Nakamura (1995). In equations (1) and (2) τ_{ij} and m_{ij}, represent the force stresses and couple stresses respectively, ε_{ij} are the conventional strain components of classical elasticity, δ_{ij} is the Kronecker delta symbol and e_{ijk} is the permutation tensor. The microrotations, ϕ_k, are independent of the conventional macrorotations, θ_k ($= e_{ijk}u_{j,i}/2$) associated with displacement components u_i. In obtaining equations (3) the four pertinent of the six independent elastic moduli, λ, μ^*, κ, α, β, and γ within (1) and (2) are reinterpreted in terms of four engineering or technical constants specified by Gauthier and Jahsman (1975) thus:-

$$E_M = \frac{\left(2\mu^* + \kappa\right)\left(3\lambda + 2\mu^* + \kappa\right)}{\left(2\lambda + 2\mu^* + \kappa\right)} \qquad (4)$$

$$v_M = \frac{\lambda}{\left(2\lambda + 2\mu^* + \kappa\right)} \qquad (5)$$

$$l_b^2 = \frac{\gamma}{2\left(2\mu^* + \kappa\right)} \qquad (6)$$

$$N^2 = \frac{\kappa}{2\left(\mu^* + \kappa\right)} \qquad (7)$$

The first two of these constants correspond to the Young's modulus and Poisson's ratio of the micropolar material. As in the classical case they can be determined by uniform unidirectional loading, the subscript M being used to differentiate them from their classical

equivalents. The third constant, l_b, termed the characteristic length in bending, recognises the intrinsically nonlocal nature of micropolar elasticity by quantifying the range of the couple stresses through their relationship to the microrotation gradients or curvatures. Lattice representations of micropolar materials indicate that the characteristic length should reflect the length scale associated with the inherent heterogeneity. From equations (3) it is easily shown that the asymmetric component, $(\tau_{xy}-\tau_{yx})/2$, of the orthogonal shear stresses, which need not be complementary, depends on the fourth constant, the coupling number, N, while the symmetric component, $(\tau_{xy}+\tau_{yx})/2$, is independent of it. The coupling number thus quantifies the level of shear stress asymmetry and thereby the degree of micropolarity exhibited by the material.

Using constitutive equations (3) Waseem et al. (2013) derives an expression for the stiffness, K, of a diametrically loaded slender micropolar ring:-

$$K = \frac{\pi E_{FM} b}{3(\pi^2 - 8)} \left(\frac{t}{R}\right)^3 \left[1 + \left(\frac{l_c}{t}\right)^2\right] \qquad (8)$$

using the approach presented previously by Huang et al. (2000) for the case of a straight beam loaded in pure bending. The thickness, t, represents the difference between the inner and outer radii of the ring while the mean radius, R, is their average and b is the breadth of the ring in the transverse direction. The additional subscript F recognises that any value of Young's modulus, E_{FM}, derived from ring stiffness is based on a flexural loading mode in which strain varies linearly rather than unidirectional one with a uniform state of strain and therefore implicitly assumes that the dependence of stress on strain remains linear across the tensile and compressive range so the modulus will be independent of the state of strain. Equation (8) assumes that bending stress varies linearly and couple stress is constant on any ring cross section. Transverse displacements and microrotations about orthogonal axes in the plane of the ring are also ignored. These assumptions were previously employed by Beveridge et al. (2013a) in deriving an analogous analytical expression for the stiffness of a straight slender beam loaded in three point bending the validity of which was then verified by both experiment and finite element analysis. It should be noted that the characteristic length, l_c, in (8) is a factor of $\sqrt{12}$ greater than l_b of (6). The term in square brackets can be regarded as a factor that corrects the stiffness of a classically elastic slender ring to account for any size effect that may be exhibited in the micropolar case. This correction implies that for rings with the same aspect ratio, R/t, stiffness should vary linearly with the reciprocal of thickness squared, $1/t^2$, and that the flexural modulus and characteristic length can be determined from the intercept and gradient of the variation respectively. The validity of the correction was again confirmed through both experimental testing and detailed finite element analysis of slender ring samples containing periodic arrays of circular voids. Moreover, the characteristic length values derived subsequently using equation (8) and the stiffness variations observed in sample sets containing voids of different diameters were found to vary with void diameter in accordance with the earlier theoretical prediction of Bigoni and Drugan (2007).

Equation (8) does not incorporate the coupling number and therefore does not distinguish between the couple stress and general micropolar cases, implying that for a slender ring there will be little difference in the size effect demonstrated in the two cases. The legitimacy of this implication is investigated further in this paper. To determine the coupling number of the perforated acrylic material Waseem et al. (2013) adopts a procedure akin to that used by

Beveridge et al. (2013a) that is based on testing less slender samples in which shear deformation is more significant. A size effect is again observed but numerical computations using a finite element approach incorporating micropolar constitutive behaviour indicate the intensity of this effect is more sensitive to the coupling number than it is in the slender sample case. The finite element procedure is thus used to identify the particular coupling number that minimizes the difference between the observed and numerically computed size effect. Interestingly, the coupling number is found to be largely independent of void size. However, the effect of changing void distribution and thereby matrix topology on the coupling number is not investigated.

Table 1 lists the characteristic length and coupling number previously quoted by Spadoni and Ruzzene (2012) for square and hexagonal lattices with each parameter depending on the length, L, and depth, d, of the beam elements that constitute the lattice. In each case the characteristic length evidently depends on the lattice spacing as reflected by element length. While the characteristic length is also weakly dependent on element aspect ratio, L/d, when the aspect ratio is large it is predicted to be a factor of approximately $\sqrt{2}$ smaller in the hexagonal case than in square case even though the offset between the centres of adjacent lattice interstices is $\sqrt{3}$ greater in a hexagonal lattice for a given element length. The coupling number also depends on the nature of the lattice and is expected to be $\sqrt{(3/2)}$ times smaller in the hexagonal case at large aspect ratio.

In the acrylic polymer matrix materials investigated by Waseem et al. (2013) the connectivity of the matrix mirrors that of a hexagonal lattice as illustrated in figure 1. However, it is unlikely that the matrix itself is adequately described by a hexagonal lattice of straight slender elements. This is evidenced by the characteristic length and coupling number values obtained for these materials which are notably different from the predictions of table 1. Nevertheless, the dependence of the coupling number on matrix connectivity as predicted for lattices according to table 1 might also be reflected in the behaviour of the acrylic matrix materials. Since this was not considered by Waseem et al. (2013) the objective of the present paper is to determine whether such dependence is observed in practice. To achieve this objective further acrylic ring samples are manufactured and tested. However, these additional samples are distinct from their predecessors in one specific aspect; the arrangement of voids within the matrix is altered such that the void centres are now located on a quadrilateral rather than a triangular array. The connectivity of the matrix thus mirrors that of a square rather than a hexagonal lattice as shown in figure 1.

3.0 Manufacture and Mechanical Testing of Ring Samples

Three sets of ring samples were manufactured from 6mm deep Oroglas® clear acrylic sheet. The first set of four samples was machined from the sheet using the computer numerically controlled (CNC) milling equipment and machining procedure employed previously. These four samples had thicknesses, t, of 3.175, 6.35, 9.525 and 15.875 mm and corresponding mean radii, R, of 25.4, 50.8, 76.2 and 127.0 mm. All four samples were thus geometrically similar with a common aspect ratio, R/t, of 8. No voids were machined into these samples, they were manufactured to enable the flexural modulus of the acrylic matrix material to be determined from their measured stiffnesses. A further set of four samples was manufactured to the same dimensions as the first set. However, in this set concentric circumferential bands of voids were also machined into the individual samples with the number of bands increasing from one in the smallest sample through two and three in the intermediate sized samples to five in the largest sample. The diameter of individual voids was 1.588 mm. However, unlike

the samples manufactured previously in which an angular offset between consecutive bands was incorporated to locate the void centres on the triangular array illustrated in figure 1 the present set of samples contained no such offset. The void centres were thereby located on a quadrilateral array as shown in figure 1. Detailed finite element analysis of a material comprised of voids located on a square array indicated that this material exhibits nearly planar isotropy and is therefore transversely isotropic. In order to bestow such behaviour on the perforated ring samples the average spacing of the voids within each circumferential band was set approximately equal to the radial spacing. In addition, the smallest sample in the present set is geometrically identical to its predecessor since it contains only a single circumferential band of voids. A third set of samples was manufactured with the same thicknesses, t, as the first two sets but with each of their mean radii, R, reduced by a factor of two. Each sample in this set thus had an aspect ratio, R/t, of 4.

Each of the samples was tested using an Instron 5969 electromechanical tensile testing machine with a 50kN load cell. Each specimen was loaded to 25N at a constant displacement rate of 1mm/min. The load cell sensitivity was adjusted to ensure accurate load measurement over the applied load range. Each sample was loaded via diametrically opposed pins placed in contact with the sample inner radius and also connected to the machine grips as shown in Figure 2. A video extensometer incorporating an infrared camera was employed to detect the position of the pins during loading. In order to determine sample displacement from the apparent strain recorded by the extensometer an initial gauge length was identified by recording the pin separation when loading commenced. Sample displacement throughout the subsequent loading could thus be determined from the product of the apparent strain recorded by the extensometer and the initial gauge length. After each sample had been loaded it was rotated by 90° relative to the pins and reloaded in order to negate any effect of manufacturing inaccuracies and obtain an average stiffness value. After loading each sample the data recorded by the testing machine acquisition system was used to graphically display the variation in load with increasing displacement. Typically a brief period of nonlinear behaviour after initial load application was followed by linear behaviour throughout the subsequent loading. Sample stiffness was determined from the gradient of the linear portion of the load displacement variation.

4.0 Finite Element Modelling of Ring Samples

One widely adopted approach to modelling heterogeneous materials is to define a representative volume element (RVE) of sufficient size that its constitutive behaviour will hopefully provide a satisfactory continuum description of the material as a whole. Heterogeneity within the volume is typically represented in detail within a finite element model which is then loaded appropriately to determine the deformation of the volume from which its constitutive behaviour can be derived. Overall material behaviour can then be inferred from volume behaviour. It is well known that resulting constitutive behaviour may depend on both the selection of a suitably sized volume and the degree of model refinement used in representing the details of heterogeneity present within the volume. In the present work overall size together with the regular nature of the heterogeneity permits modelling of the complete sample thereby avoiding any potential difficulties associated with selecting and representing a suitable RVE. All samples were therefore modelled using the proprietary finite element software package ANSYS. Mesh construction commenced by defining a quadrilateral region with two straight, radially aligned edges and two curved, circumferentially orientated edges around a particular void. This region was then divided into four subregions by radial and circumferential lines passing through the void centre. Figure 3

illustrates how the quadrilateral regions and the associated subregions were created around each of the voids within the geometric representation of the smallest sample containing only a single band of voids. Each of these subregions was then meshed using PLANE183 eight noded quadrilateral elements incorporating quadratic displacement fields. Figure 4 depicts the mesh constructed in a typical subregion. The ligament connecting the void edge to the radially aligned boundary of the subregion was apportioned into 7 element divisions. A mesh sensitivity study based on the model of a particular sample demonstrated that this level of mesh refinement was sufficient to ensure convergence of the predicted displacement field throughout the sample. Once the mesh around a particular void had been specified a mesh representing one quarter of the sample geometry was constructed by repeatedly generating the original mesh at suitable radial and circumferential increments and merging coincident nodes after each generation. Thus a structured mesh representing the quarter sample geometry of figure 3 was produced. Displacement constraints invoking symmetry were applied to the radially aligned boundaries of the quarter sample mesh as shown in figure 3. An outward radial point load was applied to the node located at the intersection of the inner edge of the mesh and one of the symmetry boundaries as also shown in figure 3. Sample stiffness was determined from the value of this load and the average radial displacement along the symmetry boundary intersecting the loading point. Stiffness was determined from this average measure of displacement to avoid introducing any error associated with local deformation at the load point itself. Radial displacement along the boundary was actually almost uniform except at the load point itself where it deviated slightly.

5.0 Results

5.1 Unperforated Ring Stiffness and Flexural Modulus of Oroglas Acrylic Polymer

The average stiffness of the four unperforated Oroglas ring samples obtained from the load displacement data produced by mechanical testing was 19.23 Nmm^{-1}. Although some variation in sample stiffness was observed this variation was independent of sample size and amounted to approximately 5% of the mean stiffness value implying that the rings behave in a classically elastic manner thus allowing equation 3 to be used to derive the flexural modulus of the homogeneous Oroglas material after prescribing l_c =0. The mean value of the flexural modulus derived accordingly was 2.99 GPa. This value compares extremely favourably with the flexural modulus of 2.94 GPa obtained previously by Waseem (2013) for a similar acrylic polymer material, Altuglas and implies that the stiffness data reported here for the perforated samples can be compared directly with data reported earlier.

5.2 Measured Stiffness of High and Low Aspect Ratio Perforated Rings

The measured stiffness of each ring in both the high and low aspect ratio sample sets is reported in Table 2. The table also lists the stiffness of each of the equivalent acrylic samples tested previously by Waseem et al. (2013) in which the void centres were located on a triangular array rather than the quadrilateral array embodied in the present samples. Two observations are immediately evident from the listed data; firstly the present samples in both the high and low aspect ratio sets exhibit the same size effect as observed previously with the stiffness increasing appreciably with reducing sample size for each set. Furthermore, the stiffness of each of the present samples is similar to its previously tested counterpart and thus the extent of the size effect is comparable.

The data listed in Table 2 are also presented in Figures 5 and 6 for the present high and low aspect ratio sample sets respectively. Each figure depicts the variation in stiffness with sample size as measured by the reciprocal of thickness squared, $1/t^2$. A linear fit has been superimposed on the experimentally determined data shown in figure 5 to indicate that the stiffness varies linearly with this sample size measure as implied by equation 8 thereby signifying that the perforated acrylic material may indeed behave as a micropolar continuum. The linear fit is subsequently used to derive values of the relevant constitutive properties, namely E_{FM} and l_c, contained within equation 8. Figure 5 also incorporates the measured stiffness data for the unperforated slender ring samples. Clearly the stiffness of each of these samples is greater than their perforated counterparts as might be expected. Moreover, the linear fit that has also been applied to these stiffness data indicates that the stiffness of the unperforated samples is evidently size independent implying that the stiffness variation in the perforated samples is a genuine effect associated with their heterogeneous microstructure rather than a consequence of other, macroscopic effects, such as the local distribution of stress in the vicinity of the load application point. The stiffness data for the low aspect ratio, R/t=4, samples displayed in figure 6 also appear to vary linearly with the sample size measure, $1/t^2$. The stiffness of each of these samples forecast by equation (8) using the constitutive properties derived from the linear fit to the high aspect ratio, R/t=8, ring data of figure 5 are also shown on figure 6. Equation (8) clearly overestimates the stiffness of each of these samples implying that they do not behave as slender rings and their increased compliance is due to unaccounted for shear deformation effects. Thus it is less straightforward to decide whether these data indicate behaviour consistent with the upper bound couple stress case or more general micropolarity since equation 8 is evidently inapplicable at this lower aspect ratio and therefore further interpretation is required.

5.3 Predicted Stiffness of High and Low Aspect Ratio Perforated Rings

The mean modulus value of 2.99 GPa, derived from experimental testing of the unperforated ring samples, together with the manufacturer's stated value of Poisson's ratio of 0.39 were assigned to each element within the FE meshes representing the matrix material of the perforated ring samples. Plane stress behaviour was assumed. Table 2 also lists the predicted stiffness of each of the current high and low aspect ratio samples. The predicted stiffness of each of the samples tested previously is also listed. It is immediately evident from the data that the predicted stiffness of each of the current samples is in close correspondence with its experimentally determined counterpart. The slight disparity in the predicted stiffness of the smallest of the present and previous samples arises from the minor difference in the measured modulus of the brand of acrylic used here and that used earlier. Some differences between measured and predicted stiffness of the current samples are also apparent with the predictions tending to be slightly higher than the measured values particularly for the larger of the low aspect ratio, R/t=4, samples. Interestingly, when the previous predictions and test data are similarly compared marginal differences are seen in these cases as well. The predicted stiffness of each of the current high and low aspect ratio samples are also shown in Figures 5 and 6 respectively. While the listed data indicate slight differences between prediction and measurement for individual samples these two figures clearly intimate that the predicted and measured extent of the overall size effect will be very similar. This similarity inspires confidence in both the accuracy of the FE models and the precision of the experimental technique in which potential error sources have apparently been negated.

6.0 Discussion

6.1 Flexural modulus and characteristic length of perforated acrylic material derived from slender, high aspect ratio, R/t=8, ring sample stiffness data

The flexural modulus and characteristic length of the perforated acrylic material were derived by using equation (8) after applying a linear fit to both the experimentally determined and predicted size effect shown in Figure 5. To maintain clarity only the fit to the measured data has been overlaid on this figure. Table 3 lists the flexural modulus values obtained from both the measured and forecast data together with the corresponding values of the characteristic length, l_c, specified according to equation (8) and its more conventional definition, l_b, given by equation (6). The consistency of the constitutive data derived from the measured and predicted size effect is significant, fitting equation (8) to the results given in table 3 is ostensibly reducing the influence of possible error associated with the measured stiffness of individual samples and consequently these derived data are strikingly similar. In addition, the values of the characteristic length, l_b, listed in table 3 are in broad agreement with the theoretical prediction of the Bigoni and Drugan (2007) analysis. Using the value of Poisson's ratio for the acrylic polymer together with the void size for the samples the value of the characteristic length predicted by this analysis is 0.71 mm. The analysis assumes both plane strain and more particularly constrained micropolar or couple stress behaviour so while these assumptions, particularly the latter, are not rigorously fulfilled in the samples the level of agreement does reinforce the credibility of the data listed in table 3.

Table 3 also lists the flexural modulus and characteristic length data obtained for the material with the triangular arrangement of perforations investigated previously. When this previous data is compared to the present data two observations are evident: the flexural modulus of the material currently under investigation is higher than that of the material considered previously, though only marginally, while the characteristic length data shows almost no difference between the two materials. While the distribution of voids in the materials differs the void volume fraction within remains essentially the same. The observations thus imply that altering the matrix topology for a fixed volume fraction has only had a slight influence on the flexural modulus and almost no bearing whatsoever on the characteristic length. As already noted lattice models indicate that the characteristic length is expected to depend on the connectivity of the elements forming the lattice. Thus while such models may predict the behaviour of periodically heterogeneous materials comprised of slender, uniform connectors it appears that these predictions cannot be extended to the behaviour of the materials considered here where the matrix cannot be represented in this manner.

6.2 Influence of coupling number on slender ring sample stiffness

The size effect predicted by FE analysis of the slender samples is once again shown in Figure 7. Three further predicted variations in sample stiffness have also been superimposed on this figure. These predictions were obtained using a higher order control volume based finite element method (CVFEM) that incorporates planar micropolar elastic constitutive behaviour. The method, developed by Beveridge et al. (2013b), is an enhanced variant of that developed by Wheel (2008), the enhancement being achieved by including quadratic rather than linear displacement fields within individual triangular elements. These were thus termed micropolar linear strain triangle (MPLST) elements. The enhanced method is particularly suited to the analysis of bending problems because of its higher order character. Furthermore, since the method incorporates micropolar behaviour the geometric details of the void array constituting

the microstructure within the acrylic material do not need to be explicitly included and therefore the internal region of each sample can be represented straightforwardly by a continuous mesh of elements. In obtaining the three additional predictions of the size effect both the modulus and characteristic length of the perforated acrylic material were set within the CVFEM procedure to those values derived from the size effect forecast by detailed FE analysis as listed in table 3. The coupling number was however varied, initially it was set to 0.99 then 0.15 and finally 0.0.

The vertical scale in figure 7 has been deliberately enlarged so that any differences between the various predictions of the size effect are visually accentuated. It is immediately evident from the figure that when the coupling number is set to 0.0 the stiffness predicted by the CVFEM is independent of the sample size and no size effect is observed thereby implying that the material is behaving in a classically elastic manner as anticipated. When $N = 0.99$ the size effect is similar to that obtained by fully detailed FE analysis although the predicted stiffness of each sample is marginally higher. However, when the coupling number is reduced radically towards the lower end of the permissible range and set to 0.15 a significant size effect is still witnessed with the stiffness of each sample being only slightly lower than the detailed FE analysis predicts. While the greatest difference is exhibited by the smallest sample the reduction in stiffness is still less than 5% in this case. Figure 8 illustrates the size effects associated with the same three values of the coupling number when representing more slender samples with an enhanced aspect ratio, R/t, of 16:1. The stiffness of each sample predicted by ANSYS where the geometric detail of the voids was explicitly accounted for are also shown on figure 8 as are the predictions of equation 8 obtained using the constitutive properties derived from the size effect exhibited by the 8:1 aspect ratio samples. Evidently the difference in the size effect seen when $N = 0.99$ and that seen in the case where $N = 0.15$ is even more marginal at the higher aspect ratio of 16:1. Furthermore figure 8 shows that the size effect remains practically unaltered even when N is reduced to 0.0625. Evidently in this case classical behaviour is only approached as the coupling number becomes vanishingly small. Thus it appears that using the approximate analytical solution, equation 8, to derive the flexural modulus and characteristic length from the stiffness of slender rings of varying size is appropriate since the size effect is almost independent of coupling number over the majority of its permissible range. Ideally the samples should be as slender as possible but in reality the use of samples with too high an aspect ratio may be impractical because of the increased likelihood of out of plane deflections, particularly in larger samples, that may potentially influence and even obscure any size effect. The agreement between the experimentally measured stiffness data and that predicted by detailed FE analysis demonstrates that the choice of a sample aspect ratio, R/t, of 8:1 actually provides a suitable compromise between the ideal of testing particularly slender samples and the practical difficulties that may be encountered when actually loading them.

6.3 Coupling number of perforated acrylic material obtained from low aspect ratio, R/t=4, ring sample stiffness data

Figure 9 shows the variation in stiffness with size predicted by the CVFEM procedure for the low aspect ratio, *R/t=4*, samples using the same three values of the coupling number used when considering the slender rings. Once again in the classical case with $N = 0.0$ no size effect is predicted while for approximate couple stress behaviour when $N = 0.99$ a marked size effect is forecast. However, when N is set to 0.15 the variation in stiffness is now predicted to lie somewhere between these bounding cases. Reducing the coupling number in this manner seems to have a more significant effect on the anticipated variation in stiffness of

the low aspect ratio, *R/t=4*, samples than their more slender counterparts for which the coupling number appeared to have little influence on the size effect. This prediction is entirely reasonable given that in the slender sample shear deformation is practically inconsequential while in the low aspect ratio, *R/t=4*, rings it will in all likelihood have a more major influence. Ascertaining the stiffness variation of the low aspect ratio, *R/t=4*, rings and comparing this to predictions thus forms the basis of a realizable means of identifying the coupling number that best describes the behaviour of the perforated acrylic material.

To identify the coupling number in this manner the CVFEM procedure was used to predict the stiffness of each of the low aspect ratio, *R/t=4*, rings across the allowable range of *N*. These predictions were then compared to the experimentally measured stiffness of each sample as well as the stiffness value ascertained from the detailed FE analysis of each ring. This comparison was made using the procedure adopted previously by Waseem et al. (2013) that was based on determining the normalised root mean square (RMS) difference or error between the predicted and actual stiffness values for the whole set of low aspect ratio, *R/t=4*, ring samples. Figure 10 illustrates how this RMS error measure varies with coupling number when the CVFEM predictions of stiffness are compared to both the experimental and FE results. Each data point on this figure in effect gives a normalized measure of the overall error in the predicted stiffness for the full set of samples. Also shown on this figure are the variations in RMS error in predicted stiffness obtained previously by Waseem et al. (2013) for the samples in which the voids were arranged in a triangular array rather than the quadrilateral arrangement featured in the current samples. Two points are immediately evident from the error variations depicted in Figure 10. Firstly, for both the current samples and those considered previously the error between the CVFEM predictions and the FEA results is noticeably less than the error between the predictions and the experimental results. In the former case constitutive properties derived from the FE results were used in generating the predictions while in the latter case properties derived from the experimental results were used. This difference in the error variations is likely to result from the inherent imprecision in the experimental results which the FE results are obviously not subject to. The second point evident from the figure is that all the error variations exhibit a minimum value which is located somewhere between $N = 0.1$ and $N = 0.2$. For both the present samples and those considered previously this minimum is more distinct for the error measure based on the difference between the CVFEM predictions and the FE results. Some slight discrepancy exists in the location of the minima identified previously for the samples with the triangular void arrangement; when predictions were compared to experimental results the minimum was located at $N = 0.125$ while comparison with the FE results located the minimum at $N = 0.175$. However, for the present samples there is no such discrepancy, both bases of comparison locate the minimum in the error variation at $N = 0.175$. In Figure 11 the stiffness predictions provided by the CVFEM procedure when $N = 0.175$ are superimposed on the detailed FE results obtained for each of the present low aspect ratio, *R/t=4*, samples. The correspondence between the CVFEM predictions and the FE results is clearly excellent for all four of the samples.

While samples with an even lower aspect ratio of 2:1 were not manufactured and tested nor considered previously finite element representations of them that explicitly incorporated the geometric details of the voids were generated using ANSYS on this occasion. The stiffness of these samples was also predicted for the allowable range of coupling numbers using the CVFEM procedure. Again, the RMS error between the CVFEM predictions and the detailed FE results were determined at each value of coupling number considered. Figure 12 illustrates the variation in this error with coupling number. A minimum error is once again

seen at around N = 0.175. Furthermore, the minimum in the error is now more obvious than when the aspect ratio was 4:1. The fact that that a unique value of this parameter has been obtained at two different aspect ratios suggests that a genuine, geometry independent, constitutive property has indeed been ascertained.

The coupling number value of 0.175 identified for the present samples with their quadrilateral void arrangement is very similar to the value obtained previously by Waseem et al. (2013) for the corresponding samples with a triangular array of voids. Hence the coupling number, like the characteristic length, appears to be insensitive to any change in matrix topology. However, lattice models indicate that alterations to topology will be accompanied by a corresponding change in this constitutive parameter in addition to the characteristic length. Thus the coupling number forecasts of lattice models while appropriate to those heterogeneous materials where the matrix is comprised of simple beam like connectors are not applicable in forecasting the behaviour of those heterogeneous materials with more elaborate matrix geometry.

7.0 Conclusions

Ring samples of a heterogeneous material consisting of circular voids within an acrylic polymer matrix were manufactured and loaded to determine the effect of sample size on stiffness. In all samples the void centres were located on a quadrilateral array. An FE analysis incorporating full geometric details of the heterogeneity was also performed for each sample. The intensity of the size effect determined for the samples from both load testing and FE analysis is remarkably similar to that found previously for comparable samples albeit with the void centres located on a triangular array. For the slender rings the size effect was interpreted within the context of planar micropolar or Cosserat elasticity theory and the value of the characteristic length constitutive parameter identified. Again, this turned out to be very similar to the value ascertained for the samples considered previously. Furthermore, additional numerical predictions imply that for slender rings the size effect is relatively insensitive to the influence to a second constitutive parameter, the coupling number, except when this parameter is very small. This vindicates the use of the closed form analytical solution for the stiffness of a slender ring for identifying the characteristic length parameter from the observed size effect.

The size effect established for a second, less slender set of ring samples enabled the parameter describing the degree of asymmetry in the shear stresses, the coupling number, to be identified. The value of this parameter was also found to be comparable to that determined previously implying that changing the topology of the material matrix has little influence on the coupling number. This result apparently contradicts the predictions obtained by static analysis of lattice models of heterogeneous materials which imply that a change in lattice connectivity should result in a more evident change in this parameter. Nevertheless, it does appear to concur with behaviour forecast in the dynamic case in which the sensitivity to topology reduces at longer wavelengths. The static loading mode employed here is arguably equivalent to the long wavelength dynamic case since the deformation field varies slowly relative to the material microstructure in both cases and hence the forecast insensitivity is being observed in practice.

References

Anderson, W.B. and Lakes, R.S., (1994), Size effects due to Cosserat elasticity and surface damage in closed-cell polymethacrylimide foam, Journal of Materials Science, 29, 6413–6419

Askar, A. and Cakmak A.S. (1968), A structural model of a micropolar continuum, International Journal of Engineering Science, 6, 583-589

Banks, C.B. and Sokolowski, M. (1968), On certain two-dimensional applications of the couple stress theory. International Journal of Solids and Structures, 4, 15–29

Bažant, Z.P. and Christensen, M. (1972), Analogy between micropolar continuum and grid frameworks under initial stress, International Journal of Solids and Structures, 8, 327-346

Beveridge, A.J., Wheel, M.A. & Nash, D.H. (2013a), The Micropolar Elastic Behaviour of Model Macroscopically Heterogeneous Materials, International Journal of Solids & Structures, 50, 246-255

Beveridge, A.J., Wheel, M.A. & Nash, D.H. (2013b), A higher order control volume based finite element method to predict the deformation of heterogeneous materials, Computers and Structures, 129, 54-62

Bigoni, D. and Drugan, W.J. (2007), Analytical derivation of Cosserat moduli via homogenization of heterogeneous elastic materials. Journal of Applied Mechanics, 74, 741–753

Chung J. and Waas A.M. (2009), The micropolar elasticity constants of circular cell honeycombs, Proceedings Royal Society London A, 465, 25-39

Dos Reis, F. and Ganghoffer, J.F., (2011), Construction of Micropolar Continua from the Homogenization of Repetitive Planar Lattices:- Chapter 9 in Mechanics of Generalized Continua (Eds. Altenbach, H., Maugin, G.A. & Erofeev, V.), Springer

Eringen, A.C., (1966), Linear theory of micropolar elasticity. Journal of Mathematics and Mechanics, 15, 909–923

Eringen, A.C., (1999), Microcontinuum Field Theories I: Foundations and Solids. Springer-Verlag New York

Gauthier, R.D. and Jahsman, W.E., (1975), A quest for micropolar elastic constants. Journal of Applied Mechanics, 42, 369–374

Gibson, L. J. and Ashby, M. F. (1997), Cellular solids, 2nd edn. Cambridge University Press

Hrennikoff A. (1941), Solution of problems of elasticity by the framework method, ASME Journal of Applied Mechanics 8, A619–A715.

Huang F.Y., Yan B.H., Yan J.L. and Yang D.U., (2000), Bending analysis of micropolar elastic beam using a 3-D finite element method. International Journal of Engineering Science, 38, 275–286

Lakes, R.S., (1983), Size effects and micromechanics of a porous solid. Journal of Materials Science, 18, 2572–2580

Lakes, R.S., (1986), Experimental microelasticity of two porous solids. International Journal of Solids and Structures, 22, 55–63

Lakes, R.S., (1995), Experimental methods for study of Cosserat elastic solids and other generalized elastic continua. in Continuum models for materials with micro-structure (Ed. Mühlhaus H.), Wiley, New York

Nakamura, S. and Lakes, R.S., (1995), Finite element analysis of Saint-Venant end effects in micropolar elastic solids. Engineering Computations, 12, 571–587

Noor, A.K. and Nemeth, M.P. (1980), Micropolar beam models for lattice grids with rigid joints, Computer Methods in Applied Mechanics and Engineeering 21, 249–263

Ostoja-Starzewski, M. (2002), Lattice models in micromechanics. ASME Journal of Applied Mechanics, 55, 35-60

Spadoni, A. and Ruzzene, M. (2012), Elasto-static micropolar behaviour of a chiral auxetic lattice, Journal of the Mechanics and Physics of Solids, 60, 156-171

Suiker, A.S.J, Metrikine, A.V. and de Borst, R., Comparison of wave propagation characteristics of the Cosserat continuum model and corresponding discrete lattice models, International Journal of Solids and Structures, 38, 1563-1583

Tekoglu, C. and Onck, P.R. (2008), Size effects in two-dimensional Voronoi foams: A comparison between generalized continua and discrete models, Journal of the Mechanics and Physics of Solids, 56, 3541-3564

Wang, A.J., and McDowell, D.L., (2004), In-plane stiffness and yield strength of periodic metal honeycombs, ASME Journal of Engineering Materials, 126, 137–156

Wang, X.L. and Stronge, W.J. (1999), Micropolar theory for two-dimensional stresses in elastic honeycomb, Proceedings Royal Society London A, 455, 2091-2116

Waseem, A., Beveridge, A. J., Wheel, M.A. and Nash, D. (2013), The influence of void size on the micropolar constitutive properties of model heterogeneous materials, European Journal of Mechanics A: Solids. 40, 148-157

Wheel, M.A., (2008), A control volume-based finite element method for plane micropolar elasticity. International Journal for Numerical Methods in Engineering, 75, 992–1006

Yang, J.F.C. and Lakes, R.S., (1982), Experimental study of micropolar and couple stress elasticity in bone in bending. Journal of Biomechanics, 15, 91–98

Short Title

Micropolar Media of Differing Topology

Topology	Characteristic Length, l_c^2	Coupling Number, N^2
Square	$L^2/24$	$1/2$
Hexagonal	$L^2(1+d^2/L^2)/48$	$(1+d^2/L^2)/(3+d^2/L^2)$

Table 1 Predicted characteristic lengths and coupling numbers for 2D lattices comprised of connectors of length L and depth d.

Ring Aspect Ratio (R/t)	Ring Mean Radius, R, (mm)	Present Quadrilateral Arrangement of Voids		Previous Triangular Arrangement of Voids [Waseem et al. (2013)]	
		Measured Stiffness (Nmm^{-1})	FEA Predicted Stiffness (Nmm^{-1})	Measured Stiffness (Nmm^{-1})	FEA Predicted Stiffness (Nmm^{-1})
8	25.4	16.588	17.388	16.248	17.160
8	50.8	13.607	13.353	13.719	13.209
8	76.2	12.629	12.697	12.399	12.477
8	127.0	12.427	12.450	11.664	12.099
4	12.7	113.600	115.843	107.880	114.079
4	25.4	94.916	95.091	90.600	92.924
4	38.1	86.813	90.899	82.634	89.007
4	63.5	80.990	89.244	82.619	87.002

Table 2 Measured and predicted stiffness of perforated ring samples with quadrilateral and triangular arrangement of voids.

	Present Quadrilateral Arrangement of Voids		Previous Triangular Arrangement of Voids [Waseem et al. (2013)]	
	Derived from Measured Stiffness Variation	Derived from FEA Predicted Stiffness Variation	Derived from Measured Stiffness Variation	Derived from FEA Predicted Stiffness Variation
Flexural Modulus, E_{FM} (Nmm^{-2})	1873.1	1850.0	1821.3	1811.4
Characteristic Length, l_c (mm)	1.88	2.08	1.93	2.11
Characteristic Length, l_b (mm)	0.54	0.60	0.56	0.61

Table 3 Flexural modulus and characteristic length values derived from measured and predicted stiffness data of slender perforated ring samples with quadrilateral and triangular void arrangements.
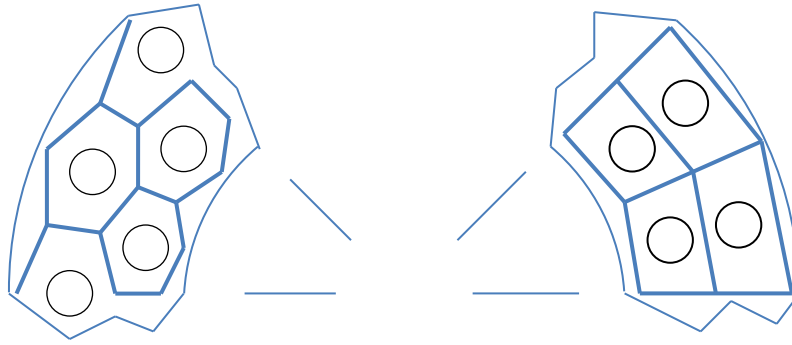
Figure 1 Sections of present (right) and previously tested (left) acrylic polymer ring samples and their analogy to quadrilateral and hexagonal lattice structures.
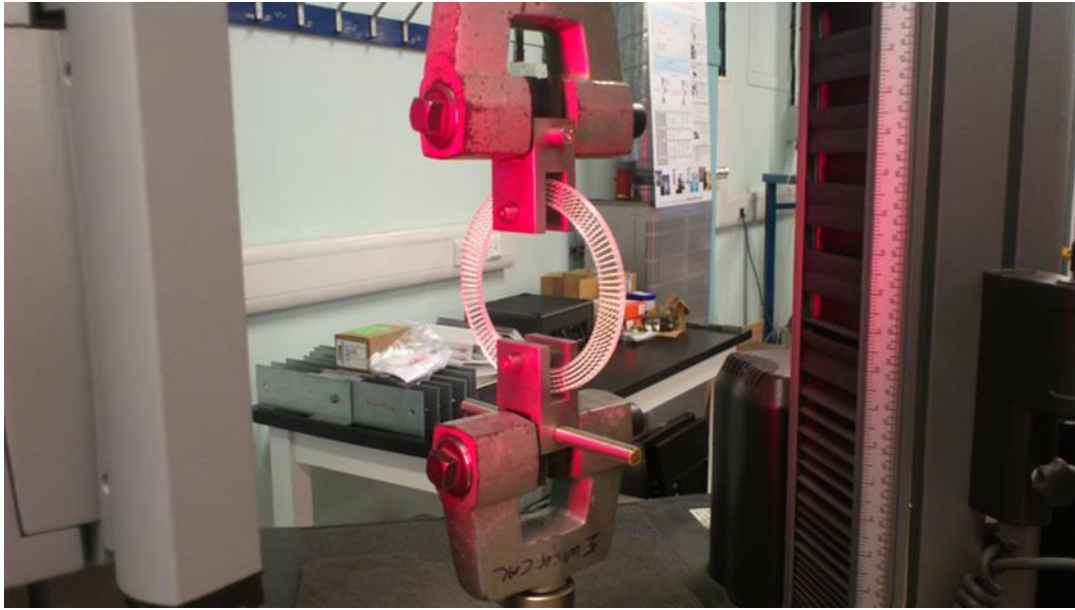
Figure 2 Mechanical loading of typical ring sample. Sample is illuminated by video extensometer which is not shown.
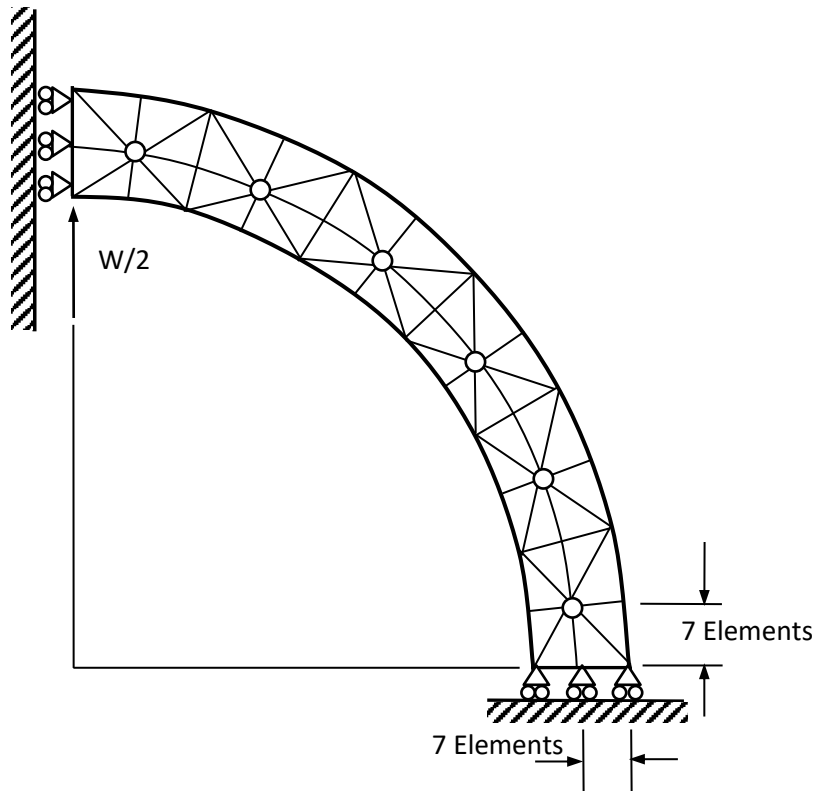
Figure 3 Geometric representation of quarter sample geometry used in generating finite element mesh with constraints also shown.
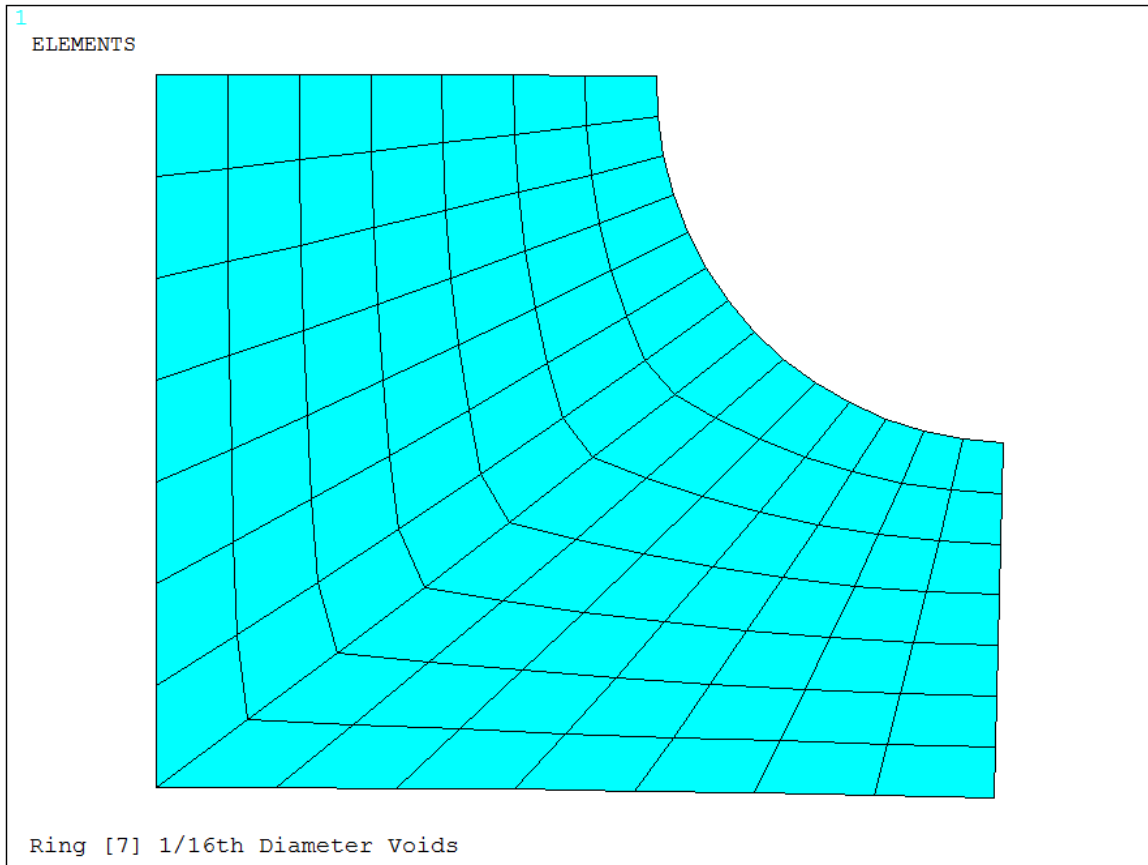
Figure 4 Finite element mesh used to represent an individual subregion of the acrylic polymer matrix adjacent to a given void within a sample.
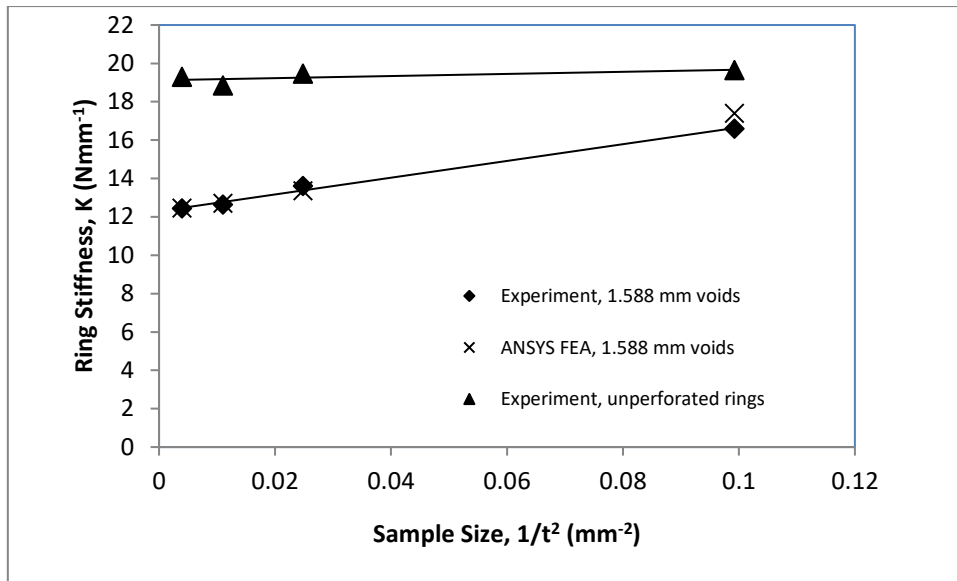
Figure 5 Measured and predicted variations in ring stiffness with sample size, $1/t^2$, for high aspect ratio, $R/t = 8.0$, rings with 1.588 mm diameter voids arranged on a quadrilateral array.
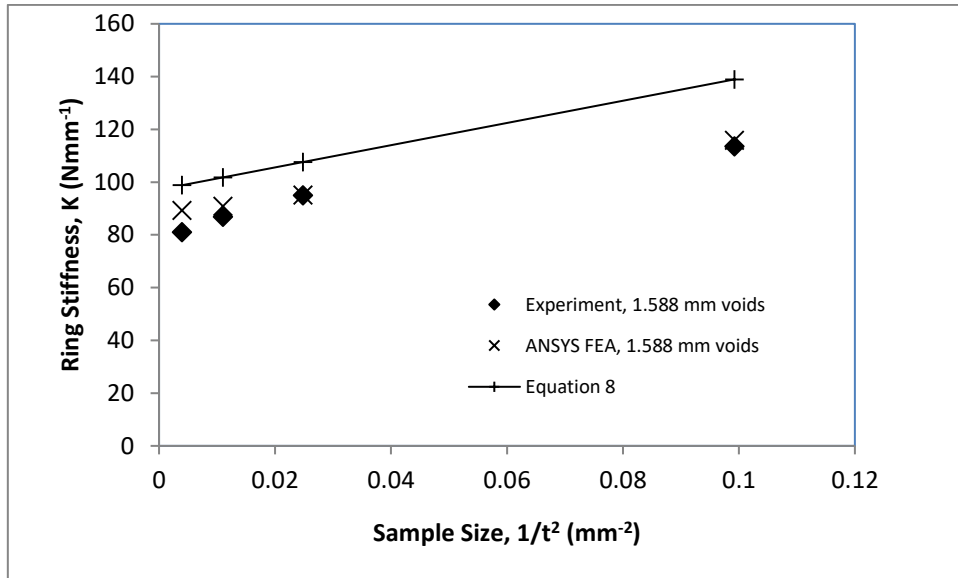
Figure 6 Measured and predicted variations in ring stiffness with sample size, $1/t^2$, for low aspect ratio, $R/t = 4.0$, rings with 1.588 mm diameter voids arranged on a quadrilateral array.
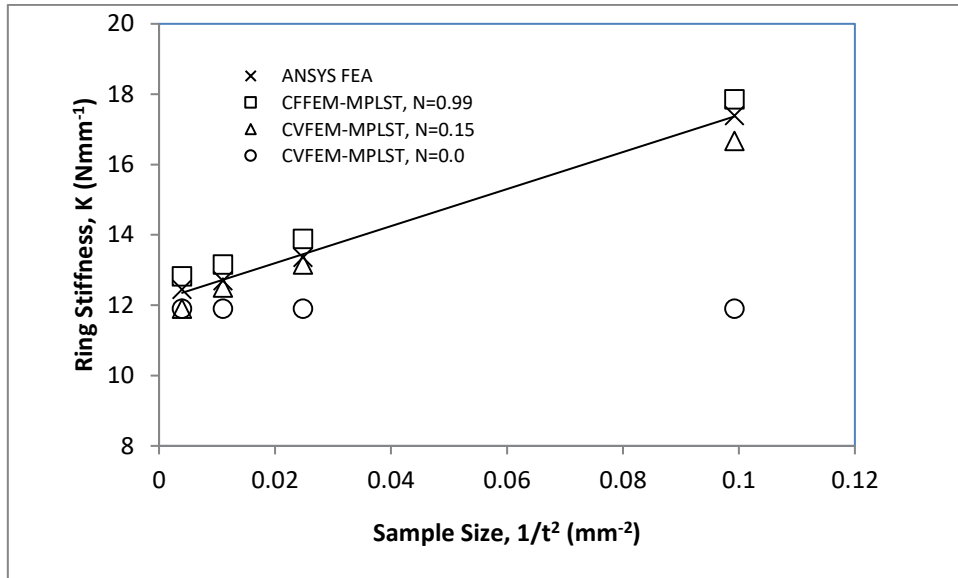
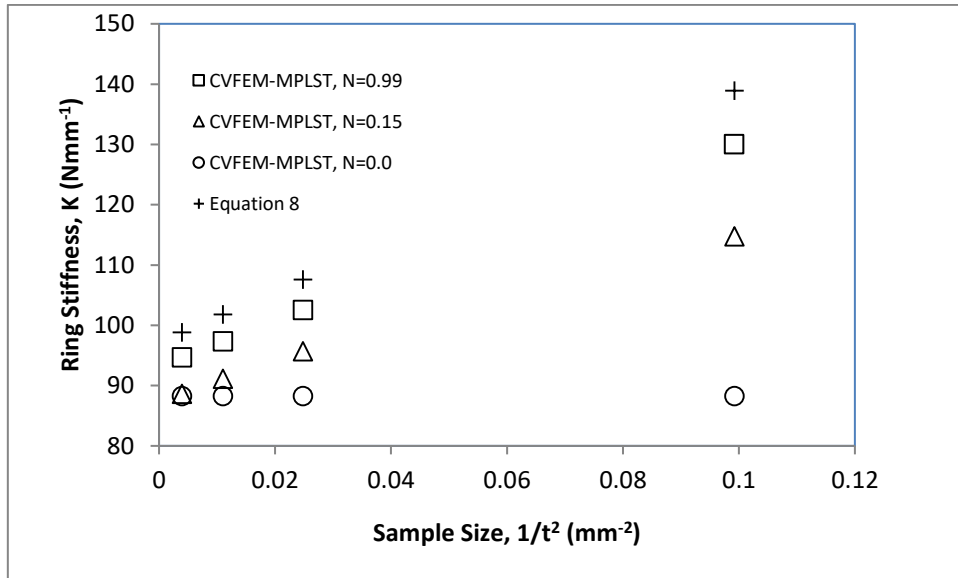Figure 7 Comparison of predicted variation in high aspect ratio, $R/t = 8.0$, ring stiffness with sample size, $1/t^2$, for coupling numbers, N, values of 0.99, 0.15 and 0.0 against detailed FEA results.
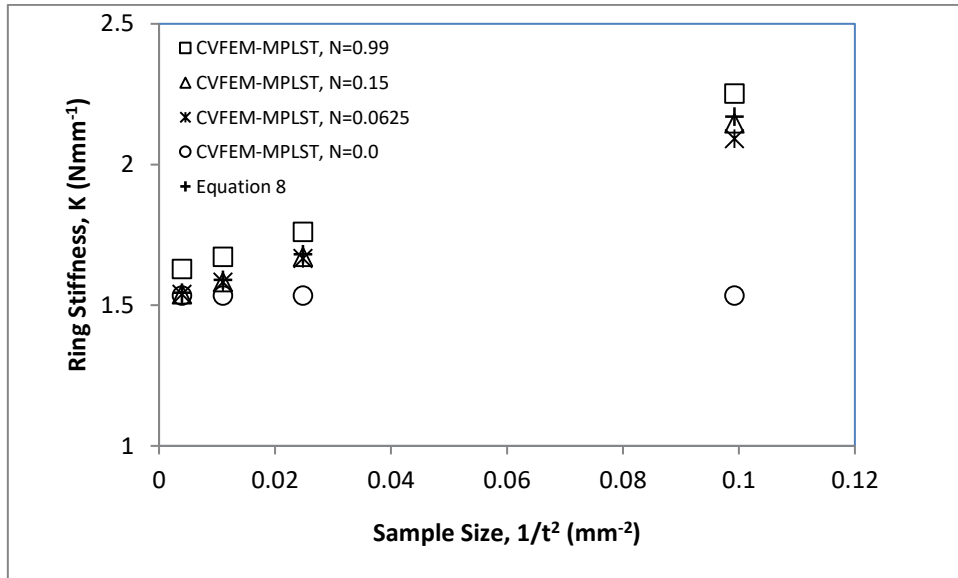
Figure 8 Predicted variation in more slender, R/t = 16.0, ring stiffness with sample size, $1/t^2$, for coupling numbers, N, values of 0.99, 0.15 and 0.0.

Figure 9 Predicted variation in low aspect ratio, R/t = 4.0, ring stiffness with sample size, $1/t^2$, for coupling numbers, N, values of 0.99, 0.15 and 0.0.
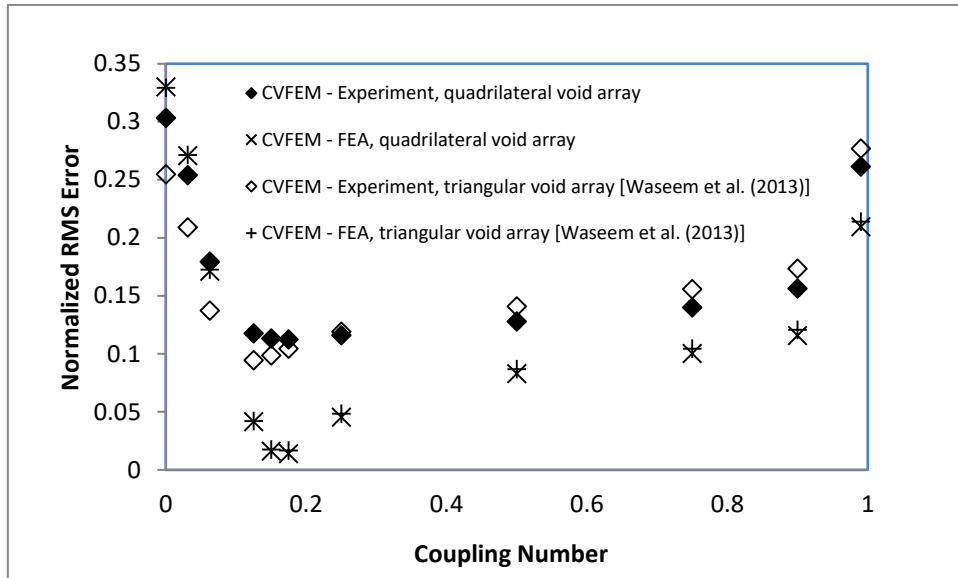
Figure 10 RMS error in predicted stiffness of all low aspect ratio, R/t = 4.0, samples with either quadrilateral or triangular void arrangements as a function of coupling number.
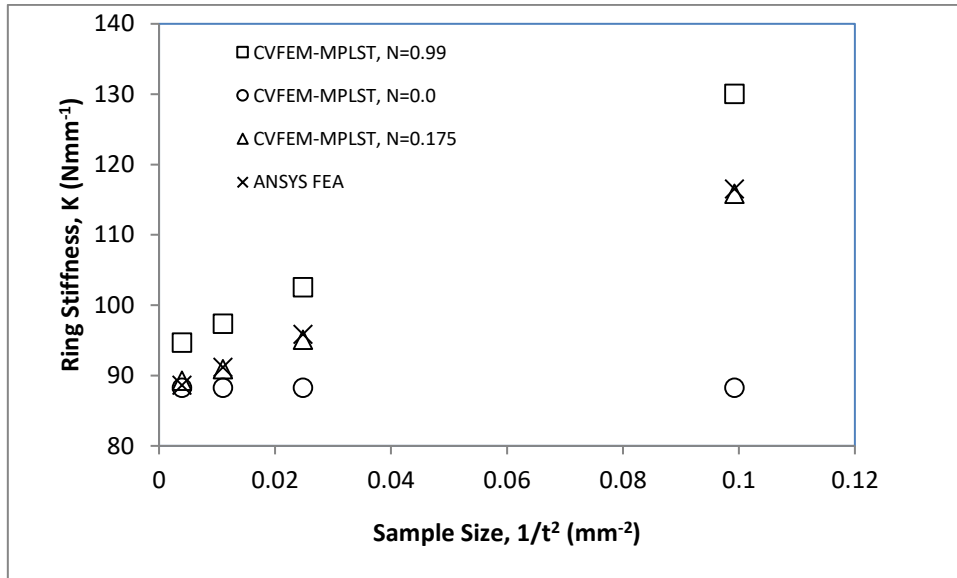
Figure 11 Comparison of predicted variation in low aspect ratio, R/t = 4.0, ring stiffness with sample size, $1/t^2$, for coupling numbers, N, values of 0.99, 0.175 and 0.0 against detailed FEA results.
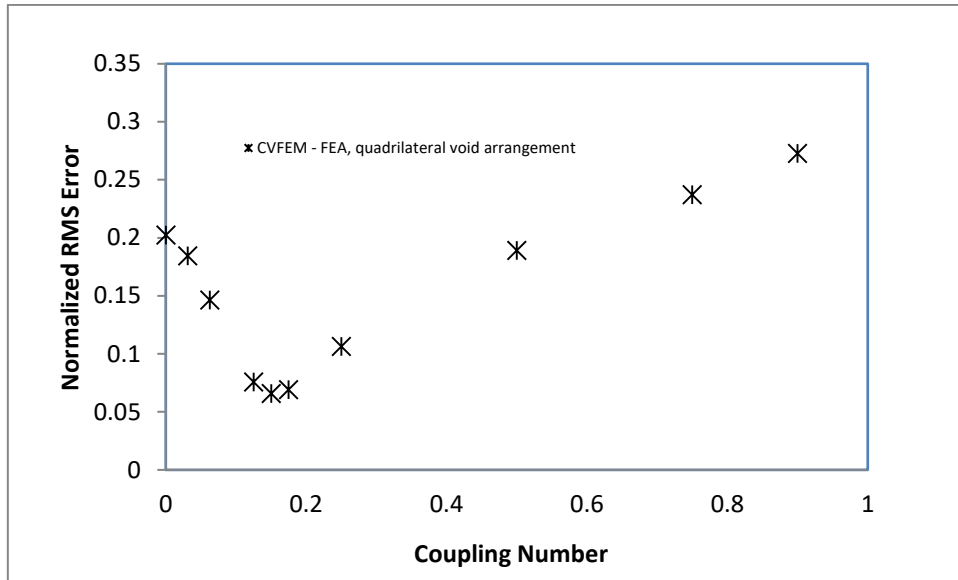
Figure 12 RMS error in predicted stiffness of aspect ratio, R/t = 2.0, samples with quadrilateral void arrangement as a function of coupling number.